Chemical Science

EDGE ARTICLE

View Article Online
View Journal | View Issue

Cite this: *Chem. Sci.*, 2015, **6**, 1498

Ultrafast photoinduced electron transfer in face-to-face charge-transfer π-complexes of planar porphyrins and hexaazatriphenylene derivatives†

Toru Aoki,[a] Hayato Sakai,[a] Kei Ohkubo,[b] Tomo Sakanoue,[c] Taishi Takenobu,*[c] Shunichi Fukuzumi*[b] and Taku Hasobe*[a]

Received 10th September 2014
Accepted 28th November 2014

DOI: 10.1039/c4sc02787f

www.rsc.org/chemicalscience

Charge-transfer (CT) π-complexes are formed between planar porphyrins and 1,4,5,8,9,12-hexaazatriphenylene (HAT) derivatives with large formation constants (*e.g.*, 10^4 M^{-1}), exhibiting broad CT absorption bands. The unusually large formation constants result from close face-to-face contact between two planar π-planes of porphyrins and HAT derivatives. The redox potentials of porphyrins and HAT derivatives measured by cyclic voltammetry indicate that porphyrins and HAT derivatives act as electron donors and acceptors, respectively. The formation of 1 : 1 CT complexes between porphyrins and HAT derivatives was examined by UV-vis, fluorescence and ^{1}H NMR measurements in nonpolar solvents. The occurrence of unprecedented ultrafast photoinduced electron transfer from the porphyrin unit to the HAT unit in the CT π-complex was observed by femtosecond laser flash photolysis measurements. A highly linear aggregate composed of a planar porphyrin and an HAT derivative was observed by transmission electron microscopy (TEM) and atomic force microscopy (AFM).

Introduction

Extensive efforts have been devoted to the construction of covalently linked electron donor–acceptor (D–A) ensembles to mimic the efficient photoinduced electron-transfer processes in the photosynthetic reaction center, which is essential to realize artificial photosynthesis.[1–9] Non-covalent interactions have also been utilized to construct more sophisticated D–A ensembles with highly ordered nanoarchitectures.[10–19] The use of non-covalent interactions has great advantage over the step-by-step synthesis of many covalent bonds due to the self-assembling features of supramolecules with non-covalent interactions. However, supramolecular D–A ensembles have a disadvantage in terms of weak interactions between electron donors and acceptors, which prohibit ultrafast photoinduced electron transfer through space.[10–19]

In order to surmount this disadvantage of supramolecular D–A ensembles, the non-covalent interactions should be strengthened by the close contact of two large planar π-planes of electron donors and acceptors. Porphyrins which have a large planar π-plane have been used as good electron donors as well as chromophores absorbing visible light in D–A ensembles (*e.g.*, electrostatic host–guest assemblies with C_{60}).[2–5,14–20] On the other hand, there are many examples of supramolecular assemblies of porphyrins, in which efficient energy transfer occurred.[20–22] Thus, porphyrins act as electron donors or energy acceptors but not electron acceptors due to the low one-electron reduction potentials. Although a variety of supramolecular D–A ensembles have been reported so far, there has been no example of a supramolecular D–A ensemble composed of porphyrins utilizing the simple close face-to-face contact for the occurrence of ultrafast photoinduced electron transfer.

Disc-like polycyclic aromatic hydrocarbon (PAH) derivatives such as triphenylene (TPh) functionalized with alkyl groups, which self-assemble into supramolecular columnar structures with hexagonal and nematic phases because of the stacking π–π interactions,[23–26] may be good candidates for use as electron acceptors to construct face-to-face complexes with planar porphyrins. In this context, 1,4,5,8,9,12-hexaazatriphenylene (HAT) derivatives have merited special attention, because these molecules possess electron deficient pyrazine units, acting as good electron acceptors.[27,28] Moreover, hexaazatriphenylene hexacarbonitrile (HAT-CN) and hexaazatriphenylene-hexacarboxy triimide (HAT-TIm) have a quite low-lying energy of the lowest unoccupied molecular orbital (LUMO) compared to

[a]*Department of Chemistry, Faculty of Science and Technology, Keio University, Yokohama, 223-8522, Japan. E-mail: hasobe@chem.keio.ac.jp*

[b]*Department of Material and Life Science, Graduate School of Engineering, Osaka University, ALCA, Japan Science and Technology Agency (JST), Suita, Osaka, 565-0871, Japan. E-mail: fukuzumi@chem.eng.osaka-u.ac.jp*

[c]*Department of Applied Physics, Waseda University, 3-4-1, Okubo, Shinjuku, Tokyo 169-8555, Japan. E-mail: takenobu@waseda.jp*

† Electronic supplementary information (ESI) available: ^{1}H, ^{13}C NMR and MALDI-TOF mass spectra, cyclic voltammograms, fluorescence spectra, fluorescence titration spectra, ^{1}H NMR titration, femtosecond laser-induced transient absorption spectral measurement data, and DFT data. See DOI: 10.1039/c4sc02787f

the pristine HAT because of the introduction of strong electron withdrawing groups such as nitrile and imide groups. The reported LUMO level of HAT-CN (−4.4 eV)[29] and the first reduction potential of HAT-TIm (−0.35 V *vs.* SCE)[30] indicate efficient electron accepting properties, which are even better than C_{60} (−0.44 V *vs.* SCE).[31] Disc shaped charge-transfer (CT) complexes of HAT-TIm with triphenylene (TPh: electron donors) have been reported recently.[32] Thus, a combination of HAT-TIm and porphyrin seems to be ideal for fulfilling an enhanced light-harvesting efficiency of chromophores throughout the solar spectrum and efficient photoinduced electron transfer. However, the photoinduced electron transfer of D–A supramolecular complexes with close contact of two large planar π-planes has yet to be examined.

We report herein ultrafast photoinduced electron transfer in supramolecular CT π-complexes formed between alkyl-substituted porphyrins and *N*-alkyl-substituted HAT-TIm with face-to-face close contact of two planar π-planes. First we examine and compare the electrochemical and photophysical properties of HAT and TPh derivatives (Chart 1). Then, the formation of strong HAT-TIm–porphyrin complexes and the ultrafast photoinduced electron transfer in the complexes including alkyl chain dependencies are discussed in detail.

Results and discussion

Synthesis

The HAT-TIm derivatives were synthesized according to the reported method by Kanakarajan and coworkers (Scheme 1).[33,34] First, compound **2** was synthesized from compound **1** under acidic conditions. Next, the dehydration condensation of compound **2** and 2,3-diaminomaleonitrile was carried out to prepare the HAT skeleton. Then, compound **4** was synthesized by acidic hydrolysis of compound **3**. To synthesize compound **5**, an HAT derivative **4** was reacted with TFA, $NaNO_2$ and AcOH, which was followed by the reaction under basic conditions. Then, compound **6** was obtained by the reaction of compound **5** with 6 N HCl at 90 °C. Compound **6** was then reacted with Ac_2O at 115 °C, which was followed by reaction with each alkyl amine. Finally, the HAT-triimide derivatives were obtained by a reaction of the crude material and thionyl chloride. HAT(COOMe)$_6$ was obtained by a reaction of compound **6** with MeOH and H_2SO_4 according to the reported method.[34] The details of C_3HAT-TIm (^{1}H, ^{13}C NMR and MALDI-TOF mass spectra) are shown in Fig. S1–S3 (ESI†). H_2P was synthesized by the reported literature[35] as shown in Scheme S1 (ESI†). Then, the synthesis of ZnP was achieved through the insertion of zinc into the porphyrin center.

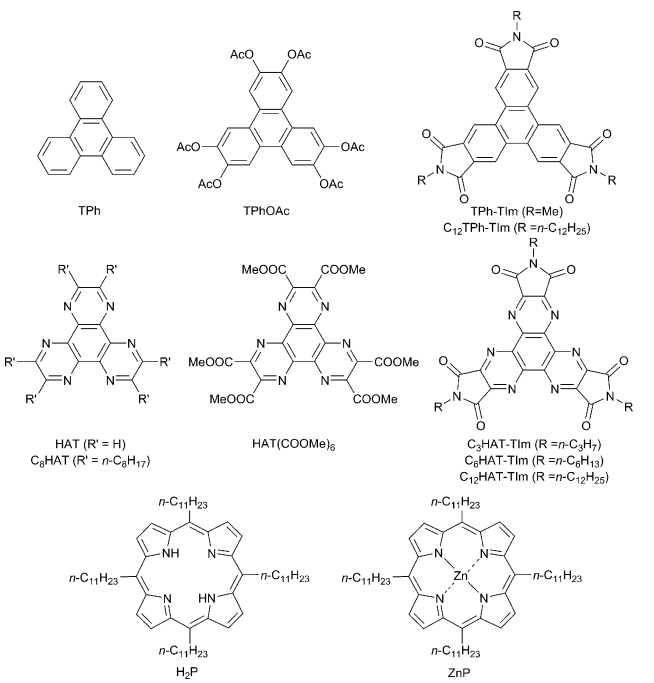

Chart 1 Chemical structures of TPh, HAT and porphyrin derivatives used in this study.

Steady-state spectroscopic measurements

Absorption spectra were measured to evaluate the electronic structures of the HAT and TPh derivatives. Fig. 1 shows the absorption spectra of TPh (spectrum a), TPhOAc (spectrum b), HAT(COOMe)$_6$ (spectrum c) and C_3HAT-TIm (spectrum d) in CH_2Cl_2. The spectrum of C_8HAT (spectrum e) is also shown for comparison although the ε value was not calculated.[36] The spectra of TPh and TPhOAc have characteristic strong peaks at around 250–270 nm, whereas the peaks of HAT(COOMe)$_6$, C_3HAT-TIm and C_8HAT have become broadened and red-shifted. According to the electrochemical measurements and DFT calculations (Table 2), the red-shift trend may result from the relatively low levels of the LUMO states by introducing electron-withdrawing groups compared to those of the HOMO states, which leads to a decrease of the HOMO–LUMO gap.[37,38]

The fluorescence spectra of TPh and TPhOAc (Fig. 2) show a fluorescence peak at *ca.* 355 nm, whereas the spectra of HAT(COOMe)$_6$ and C_3HAT-TIm exhibit extremely small intensities. Consequently, we observed the corresponding phosphorescence spectra at 77 K as shown in Fig. 3. The energies of the triplet excited states of HAT(COOMe)$_6$ and C_3HAT-TIm were determined from the phosphorescence maxima, 474 nm and 492 nm, to be 2.61 eV and 2.52 eV, respectively. Additionally, the phosphorescence lifetimes of HAT(COOMe)$_6$ and C_3HAT-TIm (77 K) were determined to be 320 ms and 280 ms, respectively (Table 1). This suggests that intersystem crossing occurs efficiently in both compounds. The absorption and emission spectra of C_6HAT-TIm and C_{12}HAT-TIm are also very similar to those of C_3HAT-TIm.

Fluorescence quantum yields

To evaluate the detailed light-emitting properties, we measured the absolute fluorescence quantum yields (Φ_F) of these derivatives and the Φ_F values are listed in Table 1. The Φ_F value of TPhOAc ($\Phi_F = 0.13$) is slightly larger than that of TPh ($\Phi_F = 0.07$), whereas the Φ_F values of HAT(COOMe)$_6$ and C_3HAT-TIm are extremely low ($\Phi_F \sim 0$). The low Φ_F values of HAT(COOMe)$_6$ and C_3HAT-TIm are consistent with the intensities of the

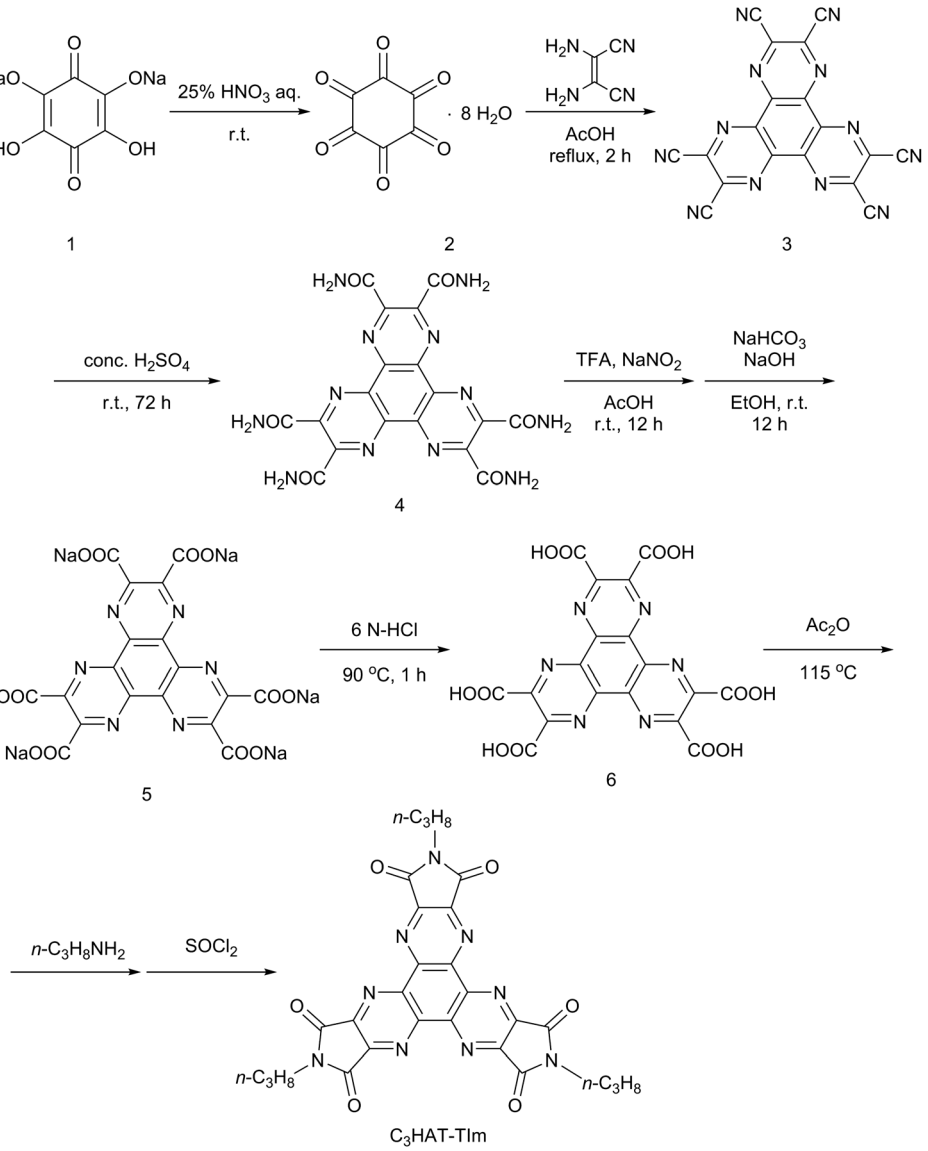

Scheme 1 Synthetic schemes of C_3HAT-TIm.

phosphorescence spectra in Fig. 3. This is attributable to the enhancement of the intersystem crossing based on spin–orbit coupling because of the introduction of carbonyl groups.[38] The low Φ_F values and the phosphorescence spectra of C_6HAT-TIm and C_{12}HAT-TIm were also similarly observed.

To further investigate and compare the fluorescence properties of TPh and TPhOAc, fluorescence lifetime measurements of these derivatives were performed. The fluorescence decays were examined in CH_2Cl_2 using a pulsed 404 nm laser light, which excited these moieties. The fluorescence lifetimes (τ_{FL}) were evaluated from a monoexponential fitting for the respective compounds and the τ_{FL} values are listed in Table 1. The τ_{FL} value of TPhOAc (9.4 ns) is much shorter than that of TPh (37 ns). To discuss the excited dynamics carefully, the net rate constants of the above two processes, fluorescence emission (k_F) and other processes (k_{Other}), were determined, as shown in Table 2. The k_F value of TPhOAc is greater than that of TPh by one order of magnitude. Additionally, in both freebase and zinc porphyrins (*e.g.*, tetraphenylporphyrin), the quantum yields of intersystem crossing (Φ_{ISC}: *ca.* 0.8–0.9) are much larger than those of the fluorescence pathways (Φ_F: *ca.* 0.05–0.10).[39b] Based on these results, we can conclude that the introduction of substituents successfully contributes to the improvement of the light-emitting property of TPh derivatives.

Electrochemical studies and DFT calculations

The electrochemical behaviors of TPh and HAT derivatives were investigated by cyclic voltammetry to examine the substituent effects on the reduction and oxidation potentials. The representative voltammograms of HAT(COOMe)$_6$ and C_6HAT-TIm in DMF or CH_2Cl_2 containing 0.10 M tetra-*n*-butylammonium hexafluorophosphate (*n*-Bu_4NPF_6) are shown in Fig. 4. The measured half-wave potentials of these compounds together with reference TPh and HAT are listed in Table 1. The first

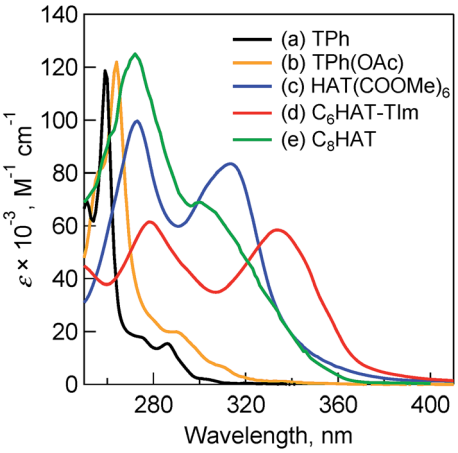

Fig. 1 Absorption spectra of (a) TPh (black), (b) TPhOAc (yellow), (c) $HAT(COOMe)_6$ (blue) and (d) C_6HAT-TIm (red) in 10 μM CH_2Cl_2. (e) Normalized absorption spectrum of C_8HAT (green) for comparison.[36]

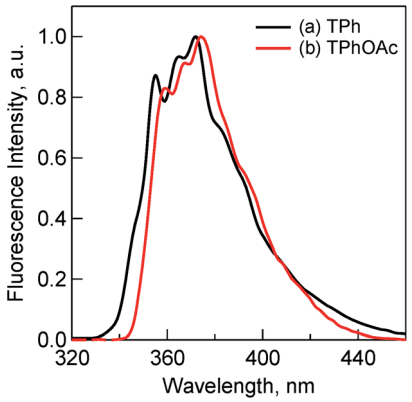

Fig. 2 Fluorescence spectra of (a) TPh (1.0 μM) (black) and (b) TPhOAc (1.0 μM) (red) in CH_2Cl_2. Excitation wavelengths are (a) 275 nm and (b) 300 nm, respectively.

Table 1 Emission parameters of TPh and HAT derivatives[a]

Compound	Φ_F	Φ_{Other}	τ_{FL}, ns	τ_{PL}, ms	$k_F \times 10^{-6}$, s^{-1}	$k_{Other} \times 10^{-7}$, s^{-1}
TPh	0.07[b]	0.93	37[b]	—	1.8	2.5
TPhOAc	0.13	0.87	9.4	—	14	9.3
$HAT(COOMe)_6$	<0.01	>0.99	—	320	—	—
C_3HAT-TIm	<0.01	>0.99	—	280	—	—

[a] τ_{FL}: fluorescence lifetime. τ_{PL}: phosphorescence lifetime (77 K). Φ_F: fluorescence emission quantum yield. Φ_{Other}: nonradiative quantum yield; $\Phi_{Other} = 1 - \Phi_F$, $k_F = \Phi_F \tau_{FL}^{-1}$, $k_{Other} = \Phi_{Other} \tau_{FL}^{-1}$. [b] Reported values.[39]

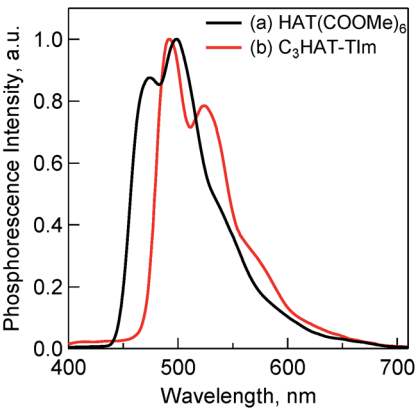

Fig. 3 Phosphorescence spectra of (a) $HAT(COOMe)_6$ (10 μM) and (b) C_3HAT-TIm (50 μM) in MeCN. The excitation wavelength is 330 nm. The measurements were performed at 77 K.

reduction (E_{red1}) and oxidation (E_{ox}) potentials of TPh were reported to be −2.42 V and +1.64 V against a saturated calomel electrode (SCE).[40,41] Similarly, we determined the first reduction potentials of TPhOAc (E_{red1} = −2.19 V), C_{12}TPh-TIm (E_{red1} = −1.21 V),[42] HAT (E_{red1} = −1.42 V),[43] $HAT(COOMe)_6$ (E_{red1} = −0.59 V) and C_6HAT-TIm (E_{red1} = −0.39 V). However, no corresponding oxidation potentials of the HAT derivatives could be determined because of the higher oxidation potentials than the solvent. The E_{red1} value of C_6HAT-TIm is quite similar to those of C_3HAT-TIm (E_{red1} = −0.39 V) and $C_{12}HAT$-TIm (E_{red1} = −0.40 V) as shown in the ESI (Fig. S4†). With increasing the number of electron-withdrawing groups such as pyrazine, COOMe, OAc and imide units, successive positive shifts of the reduction potentials were observed. In particular, the E_{red1} value of HAT-TIm is quite comparable to that of C_{60} (−0.44 V *vs.* SCE),[31] which indicates that HAT-TIm is a good electron acceptor.

Moreover, the cyclic voltammogram of C_6HAT-TIm exhibits the further reduction up to trianions, $C_6HAT\text{-}TIm^{3-}$. The HOMO and LUMO levels calculated by the DFT method (Fig. S5

Table 2 Redox potentials and HOMO–LUMO energies of TPh and HAT derivatives

Compound	E_{red1}[a]	E_{red2}[a]	E_{red3}[a]	E_{ox}[a]	HOMO[g], eV	LUMO[g], eV	gap, eV
TPh	−2.42[b]	—	—	1.64[c]	−5.89	−0.92	4.97
TPhOAc	−2.19[d]	—	—	1.63[e]	−6.20	−1.54	4.66
C_{12}TPh-TIm	−1.21[e]	—	—	—	−7.31	−3.25	4.06
HAT	−1.42[f]	−1.72[f]	—	—	−6.89	−2.16	4.73
$HAT(COOMe)_6$	−0.59	−1.08	—	—	−7.58	−3.43	4.15
C_6HAT-TIm	−0.39	−0.85	−1.21	—	−7.54	−3.63	3.91

[a] V *vs.* SCE in CH_2Cl_2. [b] Reported value in dimethylamine/THF.[40] [c] Reported value.[41] [d] Determined by differential pulse voltammetry (DPV) in THF. [e] Reported value in CH_2Cl_2.[42] [f] Reported value in MeCN.[43] [g] Calculated by B3LYP/6-31+G(d) level.

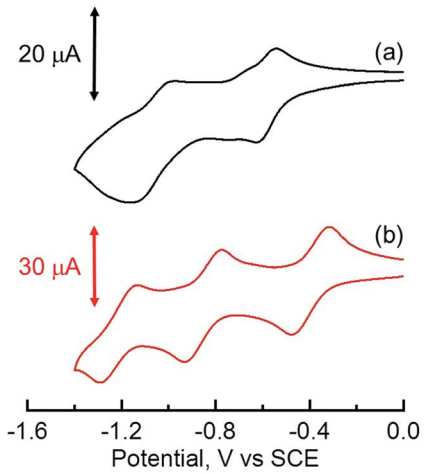

Fig. 4 Cyclic voltammograms of (a) HAT(COOMe)$_6$ in DMF and (b) C_6HAT-TIm in CH_2Cl_2 with 0.10 M n-Bu_4NPF_6 as the supporting electrolyte. Reference electrode: standard calomel electrode. Scan rate: 0.10 V s^{-1}.

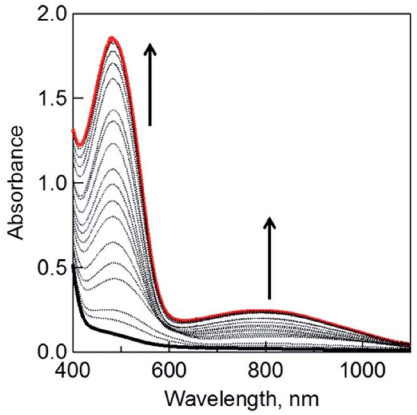

Fig. 5 The UV-vis spectral changes observed in the photoinduced electron-transfer reduction of C_3HAT-TIm (300 μM) with $(BNA)_2$ (150 μM) in deaerated CH_2Cl_2 at 298 K under photoirradiation with a xenon lamp.

and S6†) also support the above trends observed in the electrochemical data in Table 2. Namely, these shifts of the HOMO and LUMO levels are largely dependent on the electron-withdrawing nature and the number of substituents. Additionally, the LUMO of HAT-TIm is energetically low lying and doubly degenerate, and thus capable of accepting three electrons upon reduction (Fig. 4).

With regard to the porphyrin derivatives such as H_2P and ZnP, the first oxidation potentials of H_2P and ZnP were determined to be +0.78 V and +0.68 V, respectively (Fig. S7 in the ESI†). The energy level of the charge-separated state of the HAT-TIm and porphyrin (*e.g.*, ZnP) composites (*i.e.*, the HAT-TIm radical anion and the ZnP radical cation) was determined from the difference between the E_{ox} of ZnP and the E_{red1} of HAT-TIm (−0.39 V *vs.* SCE) to be 1.07 eV. This value is smaller than the excited energies of each chromophore: ~2.1 eV and ~1.5 eV for the singlet and triplet excited states of ZnP,[44] respectively, and ~3.7 eV and 2.52 eV for the singlet and triplet excited states of HAT-TIm, respectively. Thus, the photoinduced electron transfers from the excited state of ZnP to HAT-TIm and/or ZnP to the excited state of HAT-TIm are energetically favorable because the free energy changes of photoinduced electron transfer are always negative. In such a case, the combination of porphyrin and HAT-TIm units is expected to perform efficient photoinduced electron transfer to form the charge-separated state (*vide infra*).

Spectroscopic characterization of the reduced C_3HAT-TIm

When the dimeric 1-benzyl-1,4-dihydronicotinamide [$(BNA)_2$] was used as an electron donor,[45,46] irradiation of a CH_2Cl_2 solution containing $(BNA)_2$ and C_3HAT-TIm with visible light resulted in the photoinduced one-electron reduction of C_3HAT-TIm to produce C_3HAT-TIm$^{\bullet-}$. Fig. 5 shows the absorption spectral change in the photoinduced electron-transfer reduction of C_3HAT-TIm to C_3HAT-TIm$^{\bullet-}$. In this case, a new absorption band at λ_{max} = 482 nm with a broad near-IR absorption band at 800 nm appeared, corresponding to the radical anion species. The molar absorption coefficient of C_3HAT-TIm$^{\bullet-}$ was determined to be 6.2 × 10^3 M^{-1} cm^{-1} at 482 nm.

Formation constants of CT complexes between HAT-TIm and porphyrins

The CT complex formation between HAT-TIm and H_2P was examined by the absorption spectral changes (Fig. 6). The absorption of the original Soret band of H_2P at 418 nm decreased and a strong absorption peak newly appeared at around 440 nm due to the complexation of C_3HAT-TIm with H_2P in CH_2Cl_2 as shown in Fig. 6A, where the inserted figure clearly indicates formation of the typical CT π-complex between H_2P and C_3HAT-TIm. The CT complex absorption extends up to ~800 nm (ESI Fig. S8†). The Job's plot in Fig. 7 exhibits a triangle-like shape with a maximum value of 0.48, which indicates that a 1 : 1 complex (theoretical maximum: 0.50) is formed between H_2P and C_3HAT-TIm (eqn (1)).

$$H_2P + C_3\text{HAT-TIm} \overset{K}{\rightleftarrows} H_2P\cdots C_3\text{HAT-TIm} \quad (1)$$

$$(\alpha^{-1} - 1)^{-1} = K([C_3\text{HAT-TIm}] - \alpha[H_2P]_0) \quad (2)$$

$$\alpha = (A - A_0)/(A_\infty - A_0) \quad (3)$$

The formation constant (K) was determined by a linear correlation between $(\alpha^{-1} - 1)^{-1}$ and $([C_3\text{HAT-TIm}] - \alpha[H_2P]_0)$ in eqn (2) and (3), where A_0 and A are the absorbance of H_2P at 424 nm in the absence and presence of C_3HAT-TIm, and $[H_2P]_0$ is the initial concentration of H_2P. From the linear plot in the inset of Fig. 6B, the formation constant (K) of the H_2P–C_3HAT-TIm complex was determined to be 1.4 × 10^4 M^{-1} in CH_2Cl_2 (Fig. 6B). As H_2P forms the CT complex with HAT-TIm, the fluorescence emission of H_2P was quenched by intramolecular electron transfer from the singlet excited state of H_2P to C_3HAT-TIm in the complex (Fig. 8A).

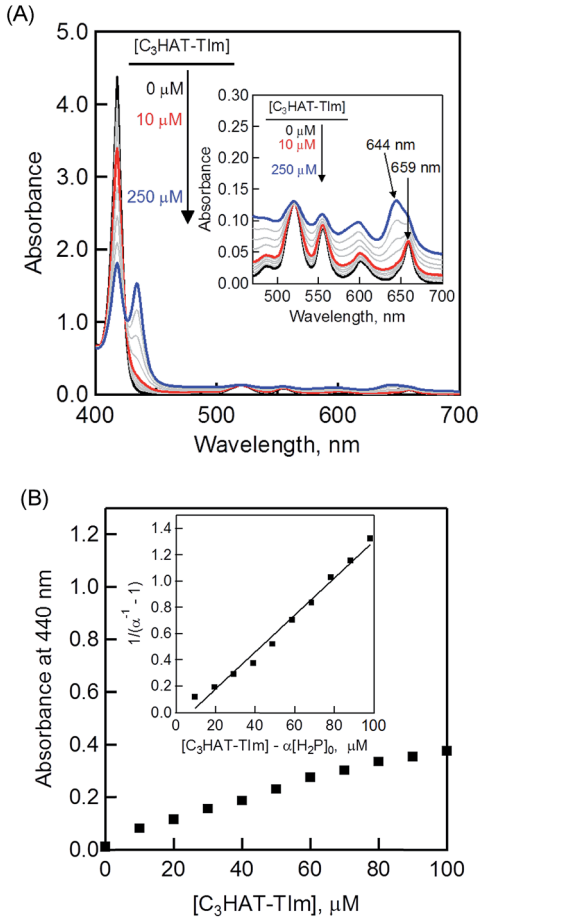

Fig. 6 (A) Absorption spectral changes of H_2P ($[H_2P] = 10$ μM) upon addition of C_3HAT-TIm (0–100 μM) in CH_2Cl_2. The inserted expanded figure indicates a broad CT absorption of the H_2P–C_3HAT-TIm complex. (B) Absorption profile at 440 nm. Inset: plot of $(\alpha^{-1} - 1)^{-1}$ *vs.* $[C_3HAT\text{-}TIm] - \alpha[H_2P]_0$.

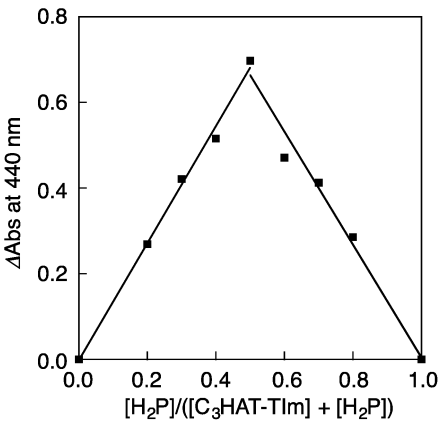

Fig. 7 The Job's plot obtained by the absorption change at 440 nm for the complex formation between H_2P and C_3HAT-TIm. The symmetric plot with maxima at 0.5 mole fraction indicates formation of the 1 : 1 complex in the present system.

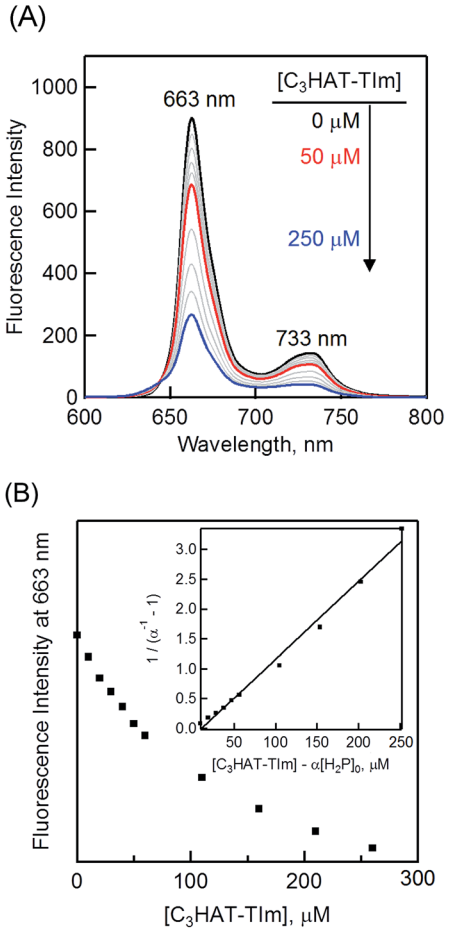

Fig. 8 (A) The fluorescence spectral changes of H_2P ($[H_2P] = 10$ μM) upon addition of increasing equivalents of C_3HAT-TIm (0–250 μM) in CH_2Cl_2. Excitation wavelength: 550 nm. (B) Plot of the fluorescence intensity *vs.* $[C_3HAT\text{-}TIm]$ at 663 nm. Inset: plot of $(\alpha^{-1} - 1)^{-1}$ *vs.* $[C_3HAT\text{-}TIm] - \alpha[H_2P]_0$ according to eqn (2) and (3).

The formation constant K of the H_2P–C_3HAT-TIm complex was determined from the changes in the fluorescence intensities at 663 nm (Fig. 8B) to be 1.3×10^4 M^{-1}, which agrees with the value determined from the absorption spectral changes in Fig. 6B.[47] The formation constants K between the porphyrins (*i.e.*, H_2P and ZnP) and the HAT-TIm derivatives are summarized in Table 3. The largest value of formation constant K was obtained for H_2P–C_6HAT-TIm as 2.1×10^4 M^{-1}. The longer alkyl chain unit may enhance the CT π-complex formation because of the additional van der Waals interaction. This is similar to that obtained for H_2P–C_{12}HAT (Fig. S9 and S10 in ESI†). When H_2P was replaced by ZnP, the formation constants became smaller (Table 3 and Fig. S11–S13 in ESI†).

Table 3 Formation constants determined by fluorescence titration of H_2P/ZnP and the HAT-TIm derivatives in CH_2Cl_2

HAT-TIm	K (H_2P), M^{-1}	K (ZnP), M^{-1}
C_3HAT-TIm	1.3×10^4	3.0×10^3
C_6HAT-TIm	2.1×10^4	6.5×10^3
C_{12}HAT-TIm	1.8×10^4	5.2×10^3

^{1}H NMR titration

The ^{1}H NMR signals of H_2P exhibit upfield shifts of β protons upon complexation with HAT-TIm as shown in Fig. 9. This is ascribed to the influence of the large porphyrin aromatic ring current. This result indicates that the two-dimensional π-structure of HAT-TIm interacts with that of H_2P.

The signals of the free H_2P and the complexed H_2P always coalesce into a single signal. This indicates that the complexation and exchange occur at a faster rate than the NMR time scale. The formation constant between H_2P and HAT-TIm was determined from the peak shifts of the β protons in the H_2P moiety using the following eqn (4):[48]

$$\Delta\delta = \frac{\Delta\delta_{max}}{-R_0}\left[\frac{[s_0]}{2} + \frac{\Sigma}{2}\left[1 - \sqrt{1 + \frac{[s_0]^2 - 2[s_0]\Psi}{\Sigma^2}}\right]\right] \quad (4)$$

$$\Sigma = [R_0] + \frac{1}{K_a} \qquad \Psi = [R_0] - \frac{1}{K_a}$$

where $\Delta\delta$ is the observed change in chemical shift, $\Delta\delta_{max}$ is the saturation value, and S_0 and R_0 are the total concentrations of guest and receptor, respectively.

A sample titration curve can be seen in the case of C_3HAT-TIm as the guest (Fig. 9B), and the formation constant was determined to be 5.1×10^3 M^{-1}. Similarly, the formation constant of H_2P–C_6HAT-TIm was determined to be 8.9×10^3 M^{-1} (Fig. S14 in the ESI†). The formation constants between the porphyrins and the HAT-TIm derivatives in $CDCl_3$ increase with increasing alkyl chain lengths as observed in the spectroscopic measurements in CH_2Cl_2. The K values in $CDCl_3$ are somewhat smaller than those in CH_2Cl_2 due to the less stabilization of CT complexes in the less polar solvent ($CDCl_3$).

DFT computational studies of supramolecular CT π-complexes

DFT calculations also support the CT π-complex formation between the porphyrin and HAT-TIm units. Fig. 10A and B show the face-to-face planar structure of the CT complex composed of ZnP and C_3HAT-TIm. The distance between the porphyrin and HAT units is found to be 3.8 Å. The calculated

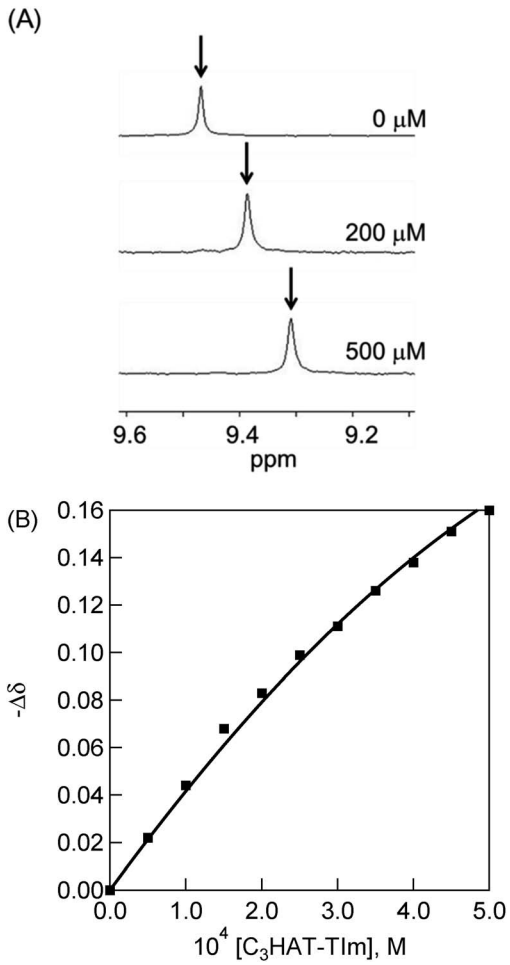

Fig. 9 (A) ^{1}H NMR titration of H_2P ([H_2P] = 500 μM) upon addition of C_3HAT-TIm (0–500 μM) in $CDCl_3$. (B) ^{1}H NMR titration curve obtained from the chemical shift changes of the β proton of H_2P by adding C_3HAT-TIm.

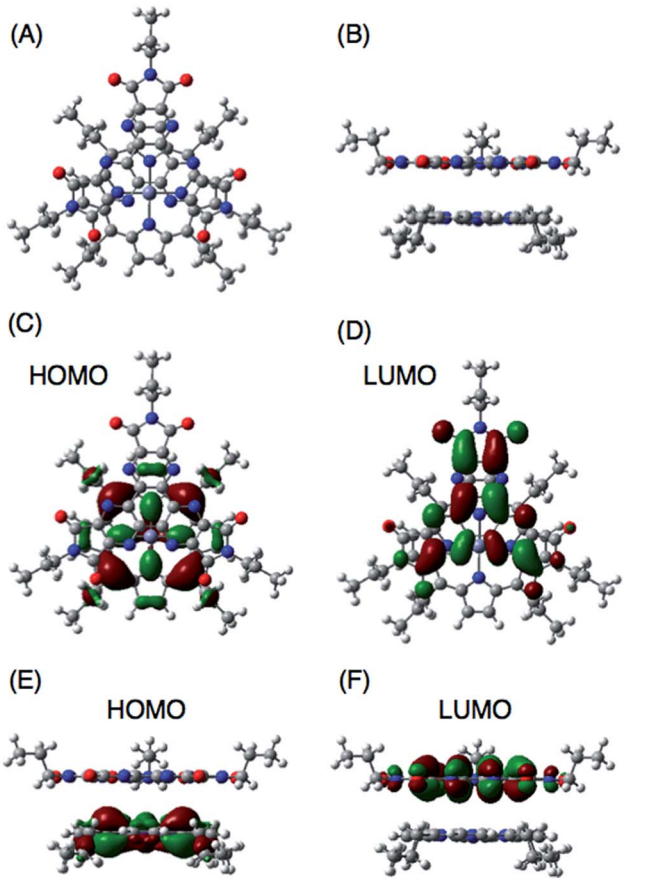

Fig. 10 B3LYP/6-31G(d) optimized structure of ZnP and C_3HAT-TIm (A and B). The HOMO and LUMO of the π-complex are shown in top view (C and D) and side view (E and F), respectively. In ZnP, the 11-carbon alkyl chains were replaced with 3-carbon chains to save computing time.

HOMO and LUMO orbitals of the CT π-complex are localized on the porphyrin and HAT-TIm units, respectively (Fig. 10C–F).[49] A similar trend was observed in the case of ZnP and C_3HAT-TIm. A TD-DFT calculation for ZnP–C_3HAT-TIm was carried out using the TD-B3LYP/6-31G(d)//B3LYP/6-31G(d) basis set to assign the absorption band at the NIR region ($\lambda_{max} = 800$ nm, Fig. 6A and Fig. S8†).[50] The calculated absorption band was obtained at 815 nm with an oscillator strength of $f = 0.172$, ascribable to charge transfer from the ZnP moiety to the C_3HAT-TIm moiety. The calculated results are shown in S15 (ESI†). We also carried out TD-DFT calculations for ZnP and C_3HAT-TIm as references, indicating that no absorption band was obtained at the NIR region (S15–S17 in the ESI†).

Ultrafast photoinduced electron transfer in CT π-complexes between porphyrins and HAT-TIm

The occurrence of ultrafast electron transfer from the singlet excited states of the porphyrins to HAT-TIm in the complexes was further confirmed by femtosecond laser-induced transient absorption measurements. The transient absorption spectra of pristine H_2P in toluene using a 430 nm laser pulse, which selectively excited only the porphyrin units, show the singlet–singlet transient absorption and fluorescence bleaching bands (*ca.* 660 nm) of H_2P (Fig. 11A). In the case of H_2P–C_3HAT-TIm, we employed a large excess concentration of C_3HAT-TIm (8 mM) relative to that of H_2P to make sure that all of the H_2P molecules formed the CT complex with C_3HAT-TIm (>99%) in Fig. 11B. The transient absorption spectra of H_2P–C_3HAT-TIm exhibit a broad absorption in the *ca.* 600–700 nm region within 1 ps after laser pulse excitation due to $H_2P^{\bullet+}$,[44,51] without fluorescence bleaching at *ca.* 660 nm (Fig. 11B). The radical anion species of C_3HAT-TIm can also be seen at around 500 nm by comparing the absorption spectrum of the reduced C_3HAT-TIm (Fig. 5).

This indicates that photoinduced charge separation occurs immediately within 1 ps upon photoexcitation of the charge-transfer without showing the singlet–singlet transient absorption due to $^1H_2P^*$. Such ultrafast charge separation is unprecedented for supramolecular electron donor–acceptor complexes,[12,17–22,52–54] resulting from a strong interaction between H_2P and a HAT-TIm derivative in the face-to-face planar structure in the CT π-complex (Fig. 10B).

The charge-recombination dynamics were monitored from the decay of the transient absorption at 630 nm due to $H_2P^{\bullet+}$ as shown in Fig. 11B. The rate constant of the charge recombination (k_{CR}) was determined to be 2.0×10^{10} s^{-1}. A similar k_{CR} value (2.2×10^{10} s^{-1}) was obtained for the H_2P–C_6HAT-TIm complex as shown in Fig. S18 (ESI†). Additionally, the transient spectra of ZnP and ZnP–C_3HAT-TIm are shown in the ESI Fig. S19.† However, photoinduced charge separation of ZnP–C_3HAT-TIm was not confirmed under our experimental set-up. This is probably attributable to the smaller formation constant ($K = 3.0 \times 10^3$ M^{-1}) than that of H_2P–C_3HAT-TIm ($K = 1.3 \times 10^4$ M^{-1}) as shown in Table 3.

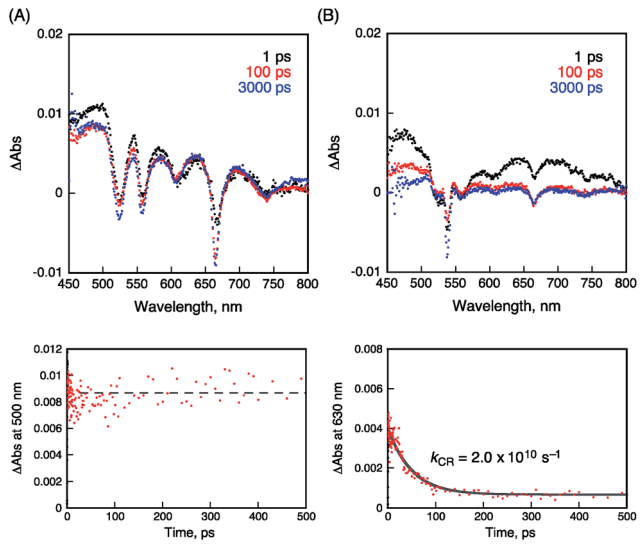

Fig. 11 Femtosecond laser-induced transient absorption spectra and corresponding time profiles of (A) H_2P and (B) H_2P–C_3HAT-TIm obtained at 1.0 ps (black), 100 ps (red) and 3000 ps (blue) after laser pulse in toluene. The time profiles were detected at 500 and 630 nm, respectively. The concentrations of H_2P and C_3HAT-TIm were 10 μM and 8.0 μM, respectively. Excitation wavelength was 430 nm.

High-order organization of the H_2P–C_3HAT-TIm complex observed by TEM and AFM

Evaporation of the solvent from a CH_2Cl_2 solution of the H_2P–C_3HAT-TIm complex resulted in high-order supramolecular organization, which was observed by TEM and AFM. The supramolecular organization patterns composed of C_3HAT-TIm and H_2P were obtained by the following method.[55] First, we optimized the experimental conditions (10 μM CH_2Cl_2 solution of C_3HAT-TIm and H_2P) by examining the concentration effect (5–50 μM) on the aggregate structures. Then, the solution (the optimized concentration: 10 μM) was simply cast onto the carbon-coated copper film (TEM grid) and dried in air. In the solvent evaporation process, the linear molecular pattern was effectively formed. The assemblies of the C_3HAT-TIm reference system were also prepared in the same manner. TEM measurements of the C_3HAT-TIm reference system without porphyrins showed many spherical assemblies (Fig. 12A), whereas aligned fibrous patterns (linear aggregates) were observed for the H_2P–C_3HAT-TIm complex (Fig. 12B). The approximate average width of the H_2P–C_3HAT-TIm assemblies was estimated to be ~200 nm. AFM measurements including the cross-sectional height information were also performed as shown in Fig. 12C. In the AFM image, we could see the surface patterning, which is very similar to the corresponding TEM images (Fig. 12B). The cross-sectional data showed the average height: 10.1 nm. Considering the chemical structure of H_2P (approximate molecular size: ~33 Å estimated by DFT) in Fig. 12D, the average height approximately corresponds to a few layers of the H_2P–C_3HAT-TIm composite units.

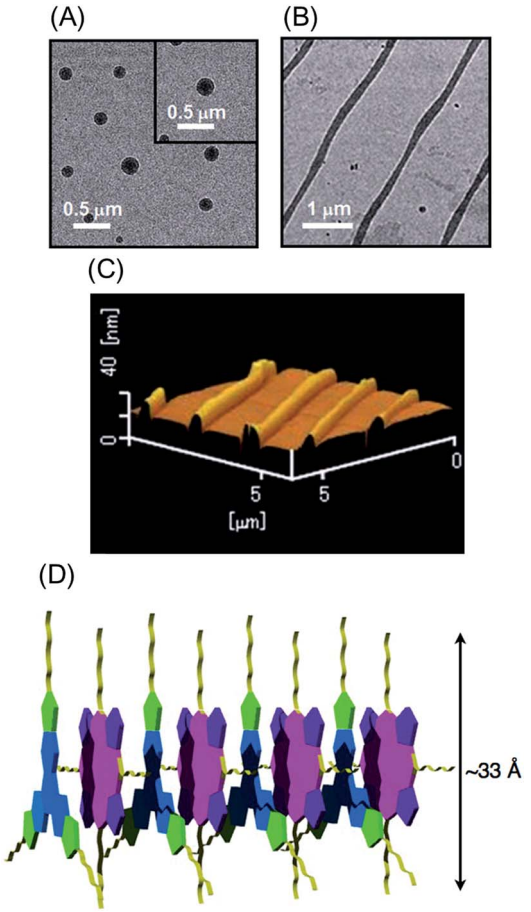

Fig. 12 TEM images of (A) the C_3HAT-TIm assembly and (B) the H_2P–C_3HAT-TIm assembly. The images were taken by drop cast of the CH_2Cl_2 solution of the components onto the grid. (C) AFM image of the H_2P–C_3HAT-TIm composites. (D) Schematic illustration of the proposed supramolecular structures between H_2P (pink/purple) and C_3HAT-TIm (blue/green).

Conclusions

The present study has demonstrated the formation of face-to-face 1 : 1 CT π-complexes between 1,4,5,8,9,12-hexaazatriphenylene (HAT) derivatives and porphyrins, which undergo ultrafast photoinduced electron transfer in which HAT derivatives with electron-withdrawing groups act as good electron acceptors. Unprecedented ultrafast charge-separated states were successfully formed by CT π-complexes. The CT π-complexes also contribute to the highly ordered patterning on the solid-state film. This simple method for molecular organization provides a new perspective for the construction and development of efficient molecular electronic and energy conversion systems.

Experimental section

General information

Triphenylene and hexaacetoxytriphenylene were purchased from Tokyo Chemical Industry (TCI). They were used after reprecipitation from dichloromethane and hexane for the spectroscopic and electrochemical measurements. All solvents and reagents of the best grade available were purchased from commercial suppliers and were used without further purification. Column flash chromatography was performed on silica gel (Kanto Chemical Silica gel 60N, 40–50 μm or 100–210 μm). We used an LC-9204 apparatus equipped with a pump (JAI PI-60, flow rate 2.5 mL min^{-1}), a UV detector (JAI UV-3740) and two columns (JAIGEL 2H and 1H, 40 × 600 mm for each). All experiments except single crystal X-ray diffraction measurements were performed at room temperature. ^{1}H NMR and ^{13}C NMR spectra were recorded on a 400 MHz spectrometer JEOL JNM-A400, JNM-Al400, or JNM-ECX 400, using the solvent peak as the reference standard, with chemical shifts given in parts per million. $CDCl_3$ was used as a solvent for NMR measurements. MALDI-TOF mass spectra were recorded on a Bruker Ultraflex.

Electrochemical measurements

Cyclic voltammograms were recorded on an Iviumstat 20 V/2.5 A potentiostat using a three electrode system. A platinum electrode was used as the working electrode. A platinum wire served as the counter electrode, and a saturated calomel electrode was used as the reference electrode. A ferrocene/ferrocenium redox couple was used as the internal standard. All the solutions were purged using nitrogen gas prior to the electrochemical and spectral measurements.

Spectroscopic measurements

UV/Vis absorption spectra were recorded on a PerkinElmer (Lambda 750) UV-VIS-NIR spectrophotometer. Fluorescence and phosphorescence emission spectra were recorded on a PerkinElmer (LS-55) spectrofluorophotometer. Fluorescence lifetimes were measured on a HORIBA Scientific time-correlated single-photon counting system (FluoroCube) with the laser light (DeltaDiode, laser diode head, 404 nm, pulse width: 100 ps) as the excitation source. Phosphorescence lifetimes were measured on a JASCO FP-8500. The absolute fluorescence quantum yields were determined by a Hamamatsu Photonics C9920-02 system equipped with an integrating sphere and a red-sensitive multichannel photodetector (PMA-12): excitation wavelength = 300 nm.

Laser flash photolysis measurements

Femtosecond laser-induced transient absorption measurements were conducted using an ultrafast source: Integra-C (Quantronix Corp.) and a commercially available optical detection system: Helios provided by Ultrafast Systems LLC. The detailed instrumentations are given in the ESI.†

Synthesis of C_3HAT-TIm

HAT **6** (0.52 mol, 0.26 g) was dissolved in acetic anhydride (15 mL), and the solution was stirred for 15 min at 115 °C. After evaporation of the solvent, the resulting solid was dissolved in acetonitrile (20 mL). Then, *n*-propylamine (12.2 mol, 1 mL) was

injected into the mixture solution with a syringe and precipitation immediately arose. The resulting solid was collected by filtration. The solid was dissolved in thionyl chloride (10 mL), and the solution was stirred for 12 h at room temperature. After the evaporation of thionyl chloride, flash column chromatography on silica gel with chloroform/methanol (1 : 1 v/v) as the eluent afforded C_3HAT-TIm. Yield: 0.23 g (77.4%). ^{1}H NMR (400 MHz, $CDCl_3$): $\delta = 3.83$ (t, $J = 7.1$ Hz, 2H, NCH_2), 1.78 (dd, $J = 7.3$ Hz, 7.6 Hz, 2H, CH_2), 1.02 (t, $J = 7.6$ Hz, 3H, CH_3); ^{13}C NMR (98.5 MHz, $CDCl_3$): $\delta = 164.1$ (C_{Ar}), 149.0 (C_{Ar}), 143.8 (C_{Ar}), 40.1 (C_{Al}), 21.3 (C_{Al}), 11.4 (C_{Al}); MALDI-TOF MS: calcd for $C_{27}H_{21}N_9O_6$: 567.16, found 567.18 [M]. ^{1}H NMR, ^{13}C NMR and MALDI-TOF mass spectra are shown in the ESI Fig. S1–S3.†

Theoretical calculations

Density functional theory (DFT) calculations of ZnP–C_3HAT-TIm, ZnP and C_3HAT-TIm were performed with Gaussian 09 (Revision A.02, Gaussian, Inc.). The calculations were performed on a 32-processor QuantumCube™ at the B3LYP/6-31G(d) level of theory.[56] Graphical outputs of the computational results were generated with the GaussView software program (ver. 3.09) developed by Semichem, Inc.[57] Electronic excitation energies and intensities were computed by the time-dependent (TD)-DFT calculation at the B3LYP/6-31G(d) level. The size of the integration grid used for all calculations was 4. In each case, 30 excited states were calculated by including all one-electron excitations within an energy window of ± 3 hartrees with respect to the HOMO–LUMO energies.

Acknowledgements

This work was partially supported by Grant-in-Aid for Scientific Research (no. 26286017 & 26620159 to T.H., no. 26620154 & 26288037 to K.O., no. 26102012 to T.T.) and the Science Research Promotion Fund from the Promotion and Mutual Aid Corporation for Private Schools from MEXT, Japan, and the Mitsubishi Foundation.

Notes and references

1 (*a*) S. Kirner, M. Sekita and D. M. Guldi, *Adv. Mater.*, 2014, **26**, 1482–1493; (*b*) J. Malig, N. Jux and D. M. Guldi, *Acc. Chem. Res.*, 2013, **46**, 53–64; (*c*) G. Bottari, G. De la Torre, D. M. Guldi and T. Torres, *Chem. Rev.*, 2010, **110**, 6768–6816.

2 (*a*) D. Gust, T. A. Moore and A. L. Moore, *Acc. Chem. Res.*, 2009, **42**, 1890–1898; (*b*) M. R. Wasielewski, *Acc. Chem. Res.*, 2009, **42**, 1910–1921; (*c*) J. Frey, G. Kodis, S. D. Straight, T. A. Moore, A. L. Moore and D. Gust, *J. Phys. Chem. A*, 2013, **117**, 607–615.

3 (*a*) S. Fukuzumi, K. Ohkubo and T. Suenobu, *Acc. Chem. Res.*, 2014, **47**, 1455–1464; (*b*) S. Fukuzumi, *Phys. Chem. Chem. Phys.*, 2008, **10**, 2283–2297; (*c*) K. Ohkubo and S. Fukuzumi, *Bull. Chem. Soc. Jpn.*, 2009, **82**, 303–315; (*d*) S. Fukuzumi, *Bull. Chem. Soc. Jpn.*, 2006, **79**, 177–195; (*e*) S. Fukuzumi, *Org. Biomol. Chem.*, 2003, **1**, 609–620.

4 (*a*) Q. Yan, Z. Luo, K. Cai, Y. Ma and D. Zhao, *Chem. Soc. Rev.*, 2014, **43**, 4199–4221; (*b*) P. D. Frischmann, K. Mahata and F. Würthner, *Chem. Soc. Rev.*, 2013, **42**, 1847–1870; (*c*) Y. K. Kang, P. M. Iovine and M. J. Therien, *Coord. Chem. Rev.*, 2011, **255**, 804–824; (*d*) B. Albinsson and J. Mårtensson, *J. Photochem. Photobiol., C*, 2008, **9**, 138–155.

5 (*a*) M. E. El-Khouly, S. Fukuzumi and F. D'Souza, *ChemPhysChem*, 2014, **15**, 30–47; (*b*) F. D'Souza and O. Ito, *Chem. Soc. Rev.*, 2012, **41**, 86–96; (*c*) S. Fukuzumi, K. Ohkubo, F. D'Souza and J. L. Sessler, *Chem. Commun.*, 2012, **48**, 9801–9815; (*d*) F. D'Souza and O. Ito, *Chem. Commun.*, 2009, 4913–4928; (*e*) R. Chitta and F. D'Souza, *J. Mater. Chem.*, 2008, **18**, 1440–1471.

6 (*a*) M. Natali, S. Campagna and F. Scandola, *Chem. Soc. Rev.*, 2014, **43**, 4005–4018; (*b*) A. Arrigo, A. Santoro, M. T. Indelli, M. Natali, F. Scandola and S. Campagna, *Phys. Chem. Chem. Phys.*, 2014, **16**, 818–826; (*c*) D. Hanss, M. E. Walther and O. S. Wenger, *Coord. Chem. Rev.*, 2010, **254**, 2584–2592.

7 (*a*) D. M. Guldi and R. D. Costa, *J. Phys. Chem. Lett.*, 2013, **4**, 1489–1501; (*b*) K. Tambara and G. D. Pantos, *Annu. Rep. Prog. Chem., Sect. B: Org. Chem.*, 2012, **108**, 186–201.

8 G. Bottari, O. Trukhina, M. Ince and T. Torres, *Coord. Chem. Rev.*, 2012, **256**, 2453–2477.

9 (*a*) S. Fukuzumi and K. Ohkubo, *Dalton Trans.*, 2013, **42**, 15846–15858; (*b*) S. Fukuzumi and K. Ohkubo, *J. Mater. Chem.*, 2012, **22**, 4575–4587; (*c*) S. Fukuzumi, T. Honda and T. Kojima, *Coord. Chem. Rev.*, 2012, **256**, 2488–2502.

10 (*a*) J. L. Sessler, B. Wang and A. Harriman, *J. Am. Chem. Soc.*, 1993, **115**, 10418–10419; (*b*) F. Wessendorf, J.-F. Gnichwitz, G. H. Sarova, K. Hager, U. Hartnagel, D. M. Guldi and A. Hirsch, *J. Am. Chem. Soc.*, 2007, **129**, 16057–16071; (*c*) H. Kar and S. Ghosh, *Chem. Commun.*, 2014, **50**, 1064–1066; (*d*) S. Verma, A. Ghosh, A. Das and H. N. Ghosh, *Chem.–Eur. J.*, 2011, **17**, 3458–3464; (*e*) S. Murphy, L. Huang and P. V. Kamat, *J. Phys. Chem. C*, 2011, **115**, 22761–22769.

11 (*a*) M. Gallego, J. Calbo, J. Aragó, R. M. Krick Calderon, F. H. Liquido, T. Iwamoto, A. K. Greene, E. A. Jackson, E. M. Pérez, E. Ortí, D. M. Guldi, L. T. Scott and N. Martín, *Angew. Chem., Int. Ed.*, 2014, **53**, 2170–2175; (*b*) K. S. Suslick and R. A. Watson, *New J. Chem.*, 1992, **16**, 633–642; (*c*) I. Duchemin and X. Blase, *Phys. Rev. B: Condens. Matter Mater. Phys.*, 2013, **87**, 245412.

12 (*a*) N. L. Bill, M. Ishida, Y. Kawashima, K. Ohkubo, Y. M. Sung, V. M. Lynch, J. M. Lim, D. Kim, J. L. Sessler and S. Fukuzumi, *Chem. Sci.*, 2014, **5**, 3888–3896; (*b*) N. L. Bill, M. Ishida, S. Bähring, J. M. Lim, S. Lee, C. M. Davis, V. M. Lynch, K. A. Nielsen, J. O. Jeppesen, K. Ohkubo, S. Fukuzumi, D. Kim and J. L. Sessler, *J. Am. Chem. Soc.*, 2013, **135**, 10852–10862; (*c*) C. M. Davis, Y. Kawashima, K. Ohkubo, J. M. Lim, D. Kim, S. Fukuzumi and J. L. Sessler, *J. Phys. Chem. C*, 2014, **118**, 13503–13513.

13 (*a*) P. Li, S. Amirjalayer, F. Hartl, M. Lutz, B. de Bruin, R. Becker, S. Woutersen and J. N. H. Reek, *Inorg. Chem.*, 2014, **53**, 5373–5383; (*b*) P. K. Poddutoori, N. Zarrabi, A. G. Moiseev, R. Gumbau-Brisa, S. Vassiliev and A. van der Est, *Chem.–Eur. J.*, 2013, **19**, 3148–3161; (*c*) E. Iengo,

G. Dan Pantosx, J. K. M. Sanders, M. Orlandi, C. Chiorboli, S. Fracasso and F. Scandola, *Chem. Sci.*, 2011, **2**, 676–685.

14 (*a*) T. Kamimura, K. Ohkubo, Y. Kawashima, H. Nobukuni, Y. Naruta, F. Tani and S. Fukuzumi, *Chem. Sci.*, 2013, **4**, 1451–1461; (*b*) H. Nobukuni, Y. Shimazaki, H. Uno, Y. Naruta, K. Ohkubo, T. Kojima, S. Fukuzumi, S. Seki, H. Sakai, T. Hasobe and F. Tani, *Chem.–Eur. J.*, 2010, **16**, 11611–11623.

15 (*a*) Y. Kawashima, K. Ohkubo, K. Mase and S. Fukuzumi, *J. Phys. Chem. C*, 2013, **117**, 21166–21177; (*b*) K. Ohkubo, Y. Kawashima and S. Fukuzumi, *Chem. Commun.*, 2012, **48**, 4314–4316; (*c*) S. Fukuzumi, K. Ohkubo, Y. Kawashima, D. S. Kim, J. S. Park, A. Jana, V. M. Lynch, D. Kim and J. L. Sessler, *J. Am. Chem. Soc.*, 2011, **133**, 15938–15941.

16 (*a*) S. Fukuzumi, T. Honda and T. Kojima, *Coord. Chem. Rev.*, 2012, **256**, 2488–2502; (*b*) M. Kanematsu, P. Naumov, T. Kojima and S. Fukuzumi, *Chem.–Eur. J.*, 2011, **17**, 12372–12384; (*c*) T. Honda, T. Nakanishi, K. Ohkubo, T. Kojima and S. Fukuzumi, *J. Am. Chem. Soc.*, 2010, **132**, 10155–10163; (*d*) T. Kojima, T. Honda, K. Ohkubo, M. Shiro, T. Kusukawa, T. Fukuda, N. Kobayashi and S. Fukuzumi, *Angew. Chem., Int. Ed.*, 2008, **47**, 6712–6716.

17 (*a*) F. D'Souza, A. N. Amin, M. E. El-Khouly, N. K. Subbaiyan, M. E. Zandler and S. Fukuzumi, *J. Am. Chem. Soc.*, 2012, **134**, 654–664; (*b*) S. Fukuzumi, K. Saito, K. Ohkubo, T. Khoury, Y. Kashiwagi, M. A. Absalom, S. Gadde, F. D'Souza, Y. Araki, O. Ito and M. J. Crossley, *Chem. Commun.*, 2011, **47**, 7980–7982; (*c*) M. E. El-Khouly, D. K. Ju, K.-Y. Kay, F. D'Souza and S. Fukuzumi, *Chem.–Eur. J.*, 2010, **16**, 6193–6202; (*d*) A. Takai, M. Chkounda, A. Eggenspiller, C. P. Gros, M. Lachkar, J.-M. Barbe and S. Fukuzumi, *J. Am. Chem. Soc.*, 2010, **132**, 4477–4489; (*e*) F. D'Souza, E. Maligaspe, K. Ohkubo, M. E. Zandler, N. K. Subbaiyan and S. Fukuzumi, *J. Am. Chem. Soc.*, 2009, **131**, 8787–8797; (*f*) F. D'Souza, N. K. Subbaiyan, Y. Xie, J. P. Hill, K. Ariga, K. Ohkubo and S. Fukuzumi, *J. Am. Chem. Soc.*, 2009, **131**, 16138–16146; (*g*) V. Bandi, M. E. El-Khouly, K. Ohkubo, V. N. Nesterov, M. E. Zandler, S. Fukuzumi and F. D'Souza, *J. Phys. Chem. C*, 2014, **118**, 2321–2332; (*h*) C. B. K. C., S. K. Das, K. Ohkubo, S. Fukuzumi and F. D'Souza, *Chem. Commun.*, 2012, **48**, 11859–11861.

18 (*a*) S. Fukuzumi and T. Kojima, *J. Mater. Chem.*, 2008, **18**, 1427–1439; (*b*) T. Kojima, T. Nakanishi, T. Honda and S. Fukuzumi, *J. Porphyrins Phthalocyanines*, 2009, **13**, 14–21; (*c*) S. Fukuzumi, T. Honda, K. Ohkubo and T. Kojima, *Dalton Trans.*, 2009, 3880–3889; (*d*) T. Kojima, K. Hanabusa, K. Ohkubo, M. Shiro and S. Fukuzumi, *Chem.–Eur. J.*, 2010, **16**, 3646–3655; (*e*) T. Honda, T. Nakanishi, K. Ohkubo, T. Kojima and S. Fukuzumi, *J. Phys. Chem. C*, 2010, **114**, 14920.

19 (*a*) P. Mondal, A. Chaudhary and S. P. Rath, *Dalton Trans.*, 2013, **42**, 12381–12394; (*b*) A. Chaudhary and S. P. Rath, *Chem.–Eur. J.*, 2012, **18**, 7404–7417; (*c*) S. Fukuzumi, I. Amasaki, K. Ohkubo, C. P. Gros, R. Guilard and J.-M. Barbe, *RSC Adv.*, 2012, **2**, 3741–3747; (*d*) S. S. Gayathri, M. Wielopolski, E. M. Pérez, G. Fernández, L. Sánchez, R. Viruela, E. Ortí, D. M. Guldi and N. Martín, *Angew. Chem., Int. Ed.*, 2009, **48**, 815–819; (*e*) M. Tanaka, K. Ohkubo, C. P. Gros, R. Guilard and S. Fukuzumi, *J. Am. Chem. Soc.*, 2006, **128**, 14625–14633.

20 (*a*) P. D. Harvey, C. Stern and R. Guilard, in *Handbook of Porphyrin Science with Applications to Chemistry, Physics, Materials Science, Engineering, Biology and Medicine*, ed. K. M. Kadish, K. M. Smith and R. Guilard, World Scientific Publishing, Singapore, 2011, vol. 11, p. 1–177; (*b*) M. K. Panda, K. Ladomenou and A. G. Coutsolelos, *Coord. Chem. Rev.*, 2012, **256**, 2601–2627; (*c*) J. Yang, M.-C. Yoon, H. Yoo, P. Kim and D. Kim, *Chem. Soc. Rev.*, 2012, **41**, 4808–4826; (*d*) V. K. Praveen, C. Ranjith, E. Bandini, A. Ajayaghosh and N. Armaroli, *Chem. Soc. Rev.*, 2014, **43**, 4222–4242.

21 (*a*) N. Aratani, D. Kim and A. Osuka, *Acc. Chem. Res.*, 2009, **42**, 1922–1934; (*b*) A. Uetomo, M. Kozaki, S. Suzuki, K.-i. Yamanaka, O. Ito and K. Okada, *J. Am. Chem. Soc.*, 2011, **133**, 13276–13279; (*c*) J.-M. Camus, S. M. Aly, D. Fortin, R. Guilard and P. D. Harvey, *Inorg. Chem.*, 2013, **52**, 8360–8368.

22 (*a*) M. Beyler, L. Flamigni, V. Heitz, J.-P. Sauvage and B. Ventura, *Photochem. Photobiol.*, 2014, **90**, 275–286; (*b*) A. Satake and Y. Kobuke, *Tetrahedron*, 2005, **61**, 13–41; (*c*) F. Hajjaj, Z. S. Yoon, M.-C. Yoon, J. Park, A. Satake, D. Kim and Y. Kobuke, *J. Am. Chem. Soc.*, 2006, **128**, 4612–4623.

23 D. Adam, P. Schuhmacher, J. Simmerer, L. Haeussling, K. Siemensmeyer, K. H. Etzbach, H. Ringsdorf and D. Haarer, *Nature*, 1994, **371**, 141–143.

24 Y. Wang, C. Zhang, H. Wu and J. Pu, *J. Mater. Chem. C*, 2014, **2**, 1667–1674.

25 (*a*) K. S. Mali, M. G. Schwab, X. Feng, K. Müllen and S. De Feyter, *Phys. Chem. Chem. Phys.*, 2013, **15**, 12495–12503; (*b*) F. Hu, Y. Gong, X. Zhang, J. Xue, B. Liu, T. Lu, K. Deng, W. Duan, Q. Zeng and C. Wang, *Nanoscale*, 2014, **6**, 4243–4249.

26 R. Nasielski-Hinkens, M. Benedek-Vamos, D. Maetens and J. Nasielski, *J. Organomet. Chem.*, 1981, **217**, 179–182.

27 R. Juárez, M. M. Oliva, M. Ramos, J. L. Segura, C. Alemán, F. Rodríguez-Ropero, D. Curcó, F. Montilla, V. Coropceanu, J. L. Brédas, Y. Qi, A. Kahn, M. C. Ruiz Delgado, J. Casado and J. T. López Navarre, *Chem.–Eur. J.*, 2011, **17**, 10312–10322.

28 G. Aragay, A. Frontera, V. Lloveras, J. Vidal-Gancedo and P. Ballester, *J. Am. Chem. Soc.*, 2013, **135**, 2620–2627.

29 T. Chiba, Y.-J. Pu, R. Miyazaki, K.-i. Nakayama, H. Sasabe and J. Kido, *Org. Electron.*, 2011, **12**, 710–715.

30 K. Pieterse, P. A. van Hal, R. Kleppinger, J. A. J. M. Vekemans, R. A. J. Janssen and E. W. Meijer, *Chem. Mater.*, 2001, **13**, 2675–2679.

31 D. Dubois, K. M. Kadish, S. Flanagan, R. E. Haufler, L. P. F. Chibante and L. J. Wilson, *J. Am. Chem. Soc.*, 1991, **113**, 4364–4366.

32 L. M. Klivansky, D. Hanifi, G. Koshkakaryan, D. R. Holycross, E. K. Gorski, Q. Wu, M. Chai and Y. Liu, *Chem. Sci.*, 2012, **3**, 2009–2014.

33 K. Kanakarajan and A. W. Czarnik, *J. Org. Chem.*, 1986, **51**, 5241–5243.

34 K. Kanakarajan and A. W. Czarnik, *J. Heterocycl. Chem.*, 1988, **25**, 1869–1872.
35 M. J. Crossley, P. Thordarson, J. P. Bannerman and P. J. Maynard, *J. Porphyrins Phthalocyanines*, 1998, **2**, 511–516.
36 Z.-G. Tao, X. Zhao, X.-K. Jiang and Z.-T. Li, *Tetrahedron Lett.*, 2012, **53**, 1840–1842.
37 S. Hirayama, H. Sakai, Y. Araki, M. Tanaka, M. Imakawa, T. Wada, T. Takenobu and T. Hasobe, *Chem.–Eur. J.*, 2014, **20**, 9081–9093.
38 K. Ida, H. Sakai, K. Ohkubo, Y. Araki, T. Wada, T. Sakanoue, T. Takenobu, S. Fukuzumi and T. Hasobe, *J. Phys. Chem. C*, 2014, **118**, 7710–7720.
39 (*a*) I. B. Berlman, in *Handbook of Fluorescence Spectra of Aromatic Molecules*, Academic Press, New York, Second Edn, 1971, p. 473; (*b*) *Handbook of Photochemistry*, ed. M. Motalti, A. Credi, L. Prodi and M. T. Gandolfi, CRC Press, Boca Raton, 3rd edn, 2006, pp. 83–157.
40 O. Reiser, B. Koenig, K. Meerholz, J. Heinze, T. Wellauer, F. Gerson, R. Frim, M. Rabinovitz and A. de Meijere, *J. Am. Chem. Soc.*, 1993, **115**, 3511–3518.
41 S. L. Mattes and S. Farid, in *Organic Photochemistry*, ed. A. Padwa, Marcel Dekker, New York, 1983, vol. 6, p. 233.
42 J. Yin, H. Qu, K. Zhang, J. Luo, X. Zhang, C. Chi and J. Wu, *Org. Lett.*, 2009, **11**, 3028–3031.
43 L. Tan-Sien-Hee and A. Kirsch-De Mesmaeker, *J. Chem. Soc., Dalton Trans.*, 1994, 3651–3658.
44 Z. Gasyna, W. R. Browett and M. Stillman, *J. Inorg. Chem.*, 1985, **24**, 2440–2447.
45 S. Fukuzumi, T. Suenobu, M. Patz, T. Hirasaka, S. Itoh, M. Fujitsuka and O. Ito, *J. Am. Chem. Soc.*, 1998, **120**, 8060–8068.
46 S. Fukuzumi, K. Ohkubo, Y. Kawashima, D. S. Kim, J. S. Park, A. Jana, V. M. Lynch, D. Kim and J. L. Sessler, *J. Am. Chem. Soc.*, 2011, **133**, 15938–15941.
47 No additional emission band was observed even though we excited the higher energy band (*i.e.*, Soret band at *ca.* 420 nm).
48 P. V. Bernhardt and E. Hayes, *J. Inorg. Chem.*, 2003, **42**, 1371–1377.
49 The stabilization energy (E_{stab}) of porphyrin and HAT-TIm was estimated from the following equation: $E_{stab} = E_{DA} - (E_D + E_A)$, where E_{DA} is the total energy of the D–A assembly, E_D and E_A are the total energies of each component. The calculated energies at the B3LYP/6-31(d) level of theory are summarized in Table S20 in the ESI.† For example, the difference of stabilization energies between ZnP–C_3HAT-TIm and ZnP–C_6HAT-TIm was 0.06 kcal mol^{-1}. Similarly, the difference was also estimated to be 0.13 kcal mol^{-1} in the case of H_2P–C_3HAT-TIm and H_2P–C_{12}HAT-TIm. These results indicate that hydrophobic interactions formed between alkyl chains can be neglected. See the following reference paper: P. R. Bangal, *J. Phys. Chem. A*, 2007, **111**, 5536–5543.
50 Dispersion-corrected calculation methods (*e.g.* WB97XD) were inconsistent with the absorption of the CT π-complex (Fig. 6A).
51 T. Hasobe, H. Imahori, P. V. Kamat, T. K. Ahn, S. K. Kim, D. Kim, A. Fujimoto, T. Hirakawa and S. Fukuzumi, *J. Am. Chem. Soc.*, 2005, **127**, 1216–1228.
52 J. L. Sessler, E. Karnas, S. K. Kim, Z. Ou, M. Zhang, K. M. Kadish, K. Ohkubo and S. Fukuzumi, *J. Am. Chem. Soc.*, 2008, **130**, 15256–15257.
53 K. Ohkubo, K. Mase, E. Karnas, J. L. Sessler and S. Fukuzumi, *J. Phys. Chem. C*, 2014, **118**, 19436.
54 T. Honda, T. Nakanishi, K. Ohkubo, T. Kojima and S. Fukuzumi, *J. Am. Chem. Soc.*, 2010, **132**, 10155–10163.
55 T. Hasobe, M. G. Rabbani, A. S. D. Sandanayaka, H. Sakai and T. Murakami, *Chem. Commun.*, 2010, **46**, 889–891.
56 *Gaussian 09, revision A.02*, Gaussian, Inc., Wallingford, CT, 2009.
57 R. Dennington II, T. Keith, J. Millam, K. Eppinnett, W. L. Hovell and R. Gilliland, *GaussView*, Semichem, Shawnee Mission, KS, 2003.